EPJ Web of Conferences **356**, 02025 (2026) https://doi.org/10.1051/epjconf/202635602025
ICC 2025

Asymmetry-dependent radius effects on the decay dynamics of Sn-isotopes formed in α-induced reactions using DCM model

Amandeep Kaur[1,*] and *S.* Sihotra[1]

[1]Department of Physics, Panjab University, Chandigarh-160014, INDIA

Abstract. Extending the results from our earlier investigation of N/Z driven structural effects on the decaying $^{110,114,120}Sn^{*}$ isotopes formed in α-induced reactions on Cd targets at common center of mass energy 15 MeV (approx.), the present work focuses on the inclusion of isospin asymmetry (I) in nuclear radius expression and consequently its effects on the decay characteristics. The isotopes under consideration possess noticeably different I=(N-Z)/A values i.e. 0.091 for lighter isotope $^{110}Sn^{*}$ and 0.167 for heavier isotope $^{120}Sn^{*}$ and hence it will be interesting to explore the influence of isotope asymmetry dependent radius R(I) on their decay behavior. The modified radius parameterization is investigated for modifications in the fragmentation potential landscape, barrier profiles and barrier positions for the decay of the chosen isotopes. A significant alteration in the barrier height and barrier position is observed for the neutron rich isotope $^{120}Sn^{*}$ when the usually used mass dependent radius R(A) is replaced with R(I). These variations in barrier profiles consequently reflect in the preformation and barrier penetration profiles. The reformulations in fragmentation behavior suggests that the minimal changes in radius terms have the tendency to induce significant variations in the structural choices of the decaying systems. Discernible modifications in the preformation probability values of alpha and other clusters are observed when isospin asymmetry is included in radius terms. This observation underlines the sensitivity of decay dynamics of nuclei formed in alpha induced reactions towards geometric corrections to radial terms. The outcome of the study emphasizes the important role of isospin asymmetry in configuring the fragmentation aspects of Sn isotopes in low energy nuclear reactions.

1 Introduction

The decay of hot and rotating nuclei populated in low-energy heavy-ion reactions have always been a subject of considerable significance in nuclear reaction dynamics, as it imparts valuable insight into the interplay between nuclear structure and decay dynamics [1–3]. In general, α-induced reactions propose a clean and controlled environment to analyze compound nucleus formation and its subsequent decay, attributed to their stable structure and well-defined excitation states. Such reactions are considered suitable for probing sophisticated structural effects that dominates fragmentation behavior [4, 5]. Over the past decades,

*e-mail: adeepkaur89@gmail.com

comprehensive research works have been devoted to comprehend the influence of mass asymmetry, excitation energy, angular momentum, and shell structure on decay characteristics such as potential energy landscapes, barrier profiles, and probabilities of cluster emission [6, 7]. With this background, isotopic chains serve as an effective laboratory for understanding the role of neutron–proton asymmetry while keeping other reaction parameters nearly constant. Specifically, Sn isotopes prove to be an excellent base due to their wide variety of isotopes and well-determined structural properties [8, 9]. Earlier studies have demonstrated that modifications in the neutron-to-proton ratio (N/Z) can predominantly affect the decay behaviour of compound systems, even when formed at comparable excitation energies. These investigations are based on mass-dependent nuclear radius parameterizations, which is successful in justifying the universal nuclear behaviors but cannot explicitly explain the isospin asymmetry effects. However, advancing experimental and theoretical studies suggests that neutron excess can induce significant variations in nuclear geometry, nuclear surface properties, and barrier characteristics, altering the decay probabilities and fragmentation paths [10].

Based on this contemplation, this work extends our previous investigations by considering isospin asymmetry dependence into the nuclear radius expression. After introducing an isospin-dependent radius expression, this work aims to estimate that minimal geometric corrections developing from neutron–proton imbalance can bring about noticeable modifications in decay behavior. Specific attention is given to the consequent modifications in potential energy landscapes, barrier heights (V_B) and positions (R_B), as well as their effect on the preformation and penetration probabilities of the clusters. The decaying systems under investigation [11], namely the $^{110,120}Sn^*$ isotopes populated via α-induced channels provide a methodical framework to explore these effects. The different behavior of the chosen isotopes on the basis of their isospin asymmetry, allows for a trasnparent assessment of the sensitivity of decay dynamics to isospin-driven geometric variations. Within this approach, the present study focuses to highlight the effect of isospin asymmetry in shaping fragmentation behavior in low-energy nuclear reactions and the theoretical analysis is carried out within the framework of the Dynamical Cluster Decay Model (DCM) [12–20]. This model treats cluster emission as a collective and dynamical process controlled by the interplay of nuclear structure and reaction dynamics. In DCM, the decay probability of a channel is factorized in terms of preformation probability of a cluster inside the compound nucleus and its subsequent tunneling/penetration through the interaction barrier. The model categorically incorporates the effects of temperature and angular momentum and provides a consistent exploration of the influence of variations in nuclear radius parameterizations on decay properties. By incorporating an isospin asymmetry–dependent radius within the DCM formulation, the present highlights the sensitivity of cluster formation and emission towards geometric correlations.

2 Methodology: The Dynamical Cluster-decay Model (DCM)

The Dynamical Cluster-decay Model (DCM) [12–20] is utilized to study the nuclear reaction dynamics focusing on the decay behavior of nuclear systems and is based on quantum mechanical fragmentation theory (QMFT). This model describes nuclear decay in terms of mass and charge asymmetry η_A and η_Z, along with relative separation R. Mass and charge asymmetry refers to the relative difference between the masses/charges of the nuclei forming the binary decay channel and is given as:

$$\eta_{mass} = \frac{A_H - A_L}{A_H + A_L} \quad and \quad \eta_{charge} = \frac{Z_H - Z_L}{Z_H + Z_L}$$

This model also considers the quadrupole deformations β_{2i} and orientations θ_i of nuclei present in the binary fragmentation channel and in the present work the orientation degree of

freedom is optimized for 'hot' configurations. DCM proceeds via two-step process: firstly, the preformation probability (P_0) of fragments of the binary decay channel preformed within the parent nucleus is determined by solving the Schrödinger equation (given below as eq. (1)) in mass (η_A) at a fixed $R = R_a$, defined by the neck formation effects. Secondly, the penetration probability (P) of the binary channel to tunnel through their interaction barrier is estimated by using the conventional WKB-approximation.

$$\left[-\frac{\hbar^2}{2\sqrt{B_{\eta\eta}}}\frac{\partial}{\partial\eta}\frac{1}{\sqrt{B_{\eta\eta}}}\frac{\partial}{\partial\eta} + V(\eta,T)\right]\psi^{\nu}(\eta) = E^{\nu}_{\eta}\psi^{\nu}(\eta), \tag{1}$$

The mass parameters ($B_{\eta\eta}$) are taken from the classical hydrodynamical model of Kröger and Scheid [21]. The resulting solution of this equation provides the preformation probability (P_0) for both ground state ($\nu = 0$) and excited states ($\nu = 1, 2, 3, ...$) and is given as:

$$P_0 = \mid \psi(\eta(A_i)) \mid^2 \sqrt{B_{\eta\eta}}\frac{2}{A_{CN}}, \tag{2}$$

The structural information enters the preformation probability through fragmentation potential $V_R(\eta,T)$, defined as:

$$V_R(\eta,T) = \sum_{i=1}^{2} BE + V_C(R,Z_i,\beta_{\lambda i},\theta_i,T) + V_P(R,A_i,\beta_{\lambda i},\theta_i,T) + V_\ell(R,A_i,\beta_{\lambda i},\theta_i,T) \tag{3}$$

Here, $\sum_{i=1}^{2} BE = \sum_{i=1}^{2} V_{LDM}(A_i,Z_i,T) + \sum_{i=1}^{2}\delta U_i \exp(-T^2/T_0^2)$ refers to the liquid drop binding energies of Seeger [22] where the T-dependence is added according to Davidson *et al.* [23] and δU is the "empirical" shell corrections from Myers and Swiatecki [24]. Note that the shell correction strongly depends on the deformations of the decaying fragments. V_C, V_P and V_ℓ are respectively, the T-dependent Coulomb, nuclear proximity and angular momentum-dependent potentials for deformed, oriented nuclei. The first turning point of the penetration path is given as the following equation and is depicted in Fig. 3, where the scattering potential (sum of V_C, V_P and V_ℓ), is plotted in terms of interaction range (R):

$$R_a = R_1(\alpha_1,T) + R_2(\alpha_2,T) + \Delta R(T) = R_t(\alpha,T) + \Delta R(T)$$

with the radius vectors

$$R_i(\alpha_i,T) = R_{0i}(T)[1 + \sum_{\lambda}\beta_{\lambda i}Y^{(0)}_{\lambda}(\alpha_i)] \tag{4}$$

with T-dependent nuclear radii R_{0i} are given by

$$R_{0i}(T) = R_{00i}(1 + 0.0007T^2). \tag{5}$$

with the mass and isospin depedent radius expressions given as

$$R_{00i} = R(A) = \left[1.28A_i^{1/3} - 0.76 + 0.8A_i^{-1/3}\right] \tag{6}$$

and

$$R_{00i} = R(I) = \left[1.256A_i^{1/3}(1 - 0.202(N_i - Z_i)/A_i)\right] \tag{7}$$

Here, ΔR assimilates the neck-formation effects. The choice of parameter R_a (equivalently, ΔR) to address the experimental data corresponds to "barrier lowering" for each decay channel, defined for each ℓ as the difference between $V_B(\ell)$ and $V(R_a,\ell)$, the barrier height and the actually used barrier, as

$$\Delta V_B = V(R_a,\ell) - V_B(\ell) \tag{8}$$

3 Results and Discussion

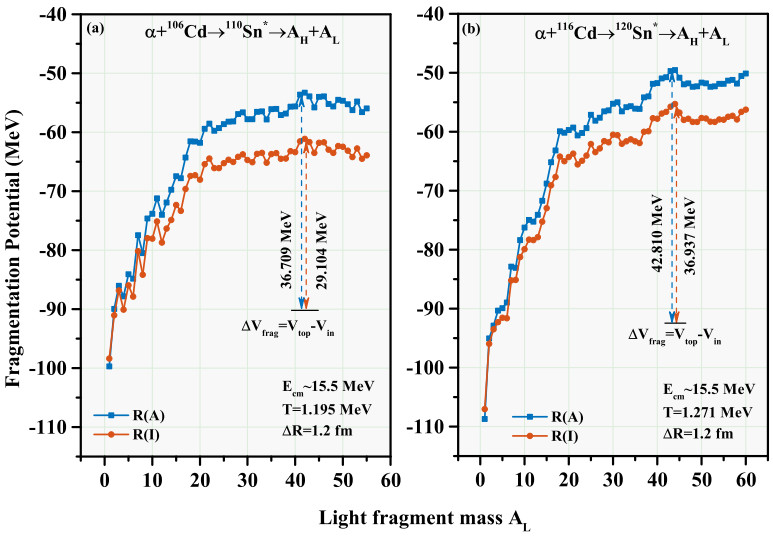

Figure 1. Behaviour of fragmentation potential in terms of light fragment mass A_L for the decay of (a) $^{110}Sn^*$ and (b) $^{120}Sn^*$ at a common center of mass energy E_{cm}~15.5 MeV (and consequently T=1.195 MeV and T=1.271 MeV respectively) and a fixed neck length parameter ΔR=1.2 fm for the choice of mass dependent R(A) and isospin dependent R(I) radius term. The driving potential ΔV_{frag}, with respect to the incoming channel, is also shown in the figure.

Figure 1 presents the fragmentation potential $V_{\rm frag}(A_L)$ for the decay of (a) $^{110}Sn^*$ and (b) $^{120}Sn^*$ at a fixed center-of-mass energy $E_{\rm c.m.} \simeq 15.5$ MeV. At this energy, the corresponding nuclear temperatures are $T = 1.195$ MeV for $^{110}Sn^*$ and $T = 1.271$ MeV for $^{120}Sn^*$. All calculations are performed at a fixed neck-length parameter $\Delta R = 1.2$ fm. The fragmentation potential, defined in Section 2 [Eq. (3)], is given by the sum of the binding energies of the fragments, shell correction terms, Coulomb potential, nuclear proximity potential, and centrifugal potential. The figure compares two different prescriptions for the nuclear radius entering the interaction potentials: the conventional mass-dependent radius $R(A)$ and the isospin-dependent radius $R(I)$. The primary objective of this comparison is to examine how the replacement of $R(A)$ by $R(I)$ influences the fragmentation structure and consequently the decay dynamics of isotopic systems with different isospin asymmetry. For this purpose, the isotopes ^{110}Sn and ^{120}Sn, having significantly different values of $I = (N - Z)/A$, are chosen. From Fig. 1, it is evident that the use of $R(I)$ induces pronounced modifications in both the magnitude and the overall structure of the fragmentation potential landscape for the two isotopic systems. The following observations can be drawn.

- A substantial change in the magnitude of the fragmentation potential is observed for fragments lying in the intermediate and heavy mass regions ($A_L > 15$). In contrast, for light fragments with $A_L = 1$–4, which constitute the light-particle emission region of primary interest, the variation in magnitude due to the change in radius prescription is comparatively small. This behavior is consistently observed for both $^{110}Sn^*$ and $^{120}Sn^*$, indicating that the isospin dependence of the radius predominantly affects heavier fragment configurations.

- The incorporation of the isospin-dependent radius $R(I)$ leads to an overall reduction in the magnitude of the fragmentation potential as compared to that obtained using $R(A)$. Physically, this reduction implies a lowering of the effective potential energy landscape governing the mass-asymmetric decay configurations. As a consequence, the relative stability of certain fragment partitions is enhanced, which is expected to influence both the preformation probabilities and the barrier penetration characteristics of the decay fragments for the chosen isotopes.
- The effect of the radius prescription is further quantified through the driving potential, defined as

$$\Delta V_{\rm frag} = V_{\rm top} - V_{\rm in}, \tag{9}$$

  where $V_{\rm top}$ denotes the fragmentation potential corresponding to the top of the potential curve and $V_{\rm in}$ represents the potential at the entrance (incoming) channel. When $R(A)$ is replaced by $R(I)$, the driving potential for ^{110}Sn* decreases from 36.709 MeV to 29.104 MeV, while for ^{120}Sn* it reduces from 42.810 MeV to 36.937 MeV. This reduction in $\Delta V_{\rm frag}$ signifies a weaker driving force for mass rearrangement, suggesting an enhanced probability for the system to explore a broader range of mass partitions during the decay process, especially in neutron-rich systems.
- An additional notable feature is the modification of the relative depth and position of the minima in the fragmentation potential when $R(I)$ is employed. These changes reflect the sensitivity of shell-driven structure effects to the isospin-dependent geometry of the interacting fragments, particularly for the neutron-rich isotope ^{120}Sn*. Such modifications are expected to play a crucial role in determining the isotopic dependence of decay observables within the dynamical cluster-decay model.

Hence, the present analysis clearly demonstrates that the inclusion of an isospin-dependent radius significantly alters the fragmentation potential landscape for both ^{110}Sn* and ^{120}Sn*. The observed reduction in the overall potential magnitude and driving potential highlights the importance of isospin asymmetry in governing the decay dynamics of hot and rotating nuclei, particularly for neutron-rich systems.

In Fig. 2, we present the other key ingredients of the Dynamical Cluster-decay Model (DCM), namely the preformation probability P_0 and the penetration probability P, whose combined contribution determines the decay cross-sections within the DCM framework. Figures 2(a) and 2(d) show the angular momentum dependence of the preformation probability P_0 for the α-decay channels ^{110}Sn$^* \rightarrow {}^{106}$Cd+α and ^{120}Sn$^* \rightarrow {}^{116}$Cd+α, respectively, for both choices of the radius parameterization, $R(A)$ and $R(I)$. For both isotopic systems, the preformation probability initially increases with angular momentum and attains a maximum at a certain ℓ value, followed by a rapid fall to negligible or zero values. Using both radius prescriptions, the maximum in P_0 occurs around $\ell \simeq 60\hbar$ for ^{110}Sn* and $\ell \simeq 75\hbar$ for ^{120}Sn*. Beyond these values, the centrifugal effects dominate and suppress the cluster preformation. The angular momentum at which P_0 becomes negligible is identified as $\ell_{\rm max}$. For the mass-dependent radius $R(A)$ (blue curves), $\ell_{\rm max}$ is found to be $69\hbar$ for ^{110}Sn* and $81\hbar$ for ^{120}Sn*. When $R(A)$ is replaced by the isospin-dependent radius $R(I)$ (orange curves), the overall magnitude of the preformation probability is noticeably enhanced for both systems, reflecting an increased structural favorability for α-cluster formation. The corresponding $\ell_{\rm max}$ values remain nearly unchanged, being $68\hbar$ for ^{110}Sn* and $81\hbar$ for ^{120}Sn*. It is also evident that higher angular momentum states are populated in the heavier isotope ^{120}Sn* as compared to ^{110}Sn*, independent of the choice of radius parameterization. Figures 2(b) and 2(e) display the penetration probability P as a function of angular momentum for ^{110}Sn* and ^{120}Sn*, respectively. For the $R(A)$ prescription (blue curves), the penetrability becomes non-zero at $\ell \simeq 20\hbar$ for

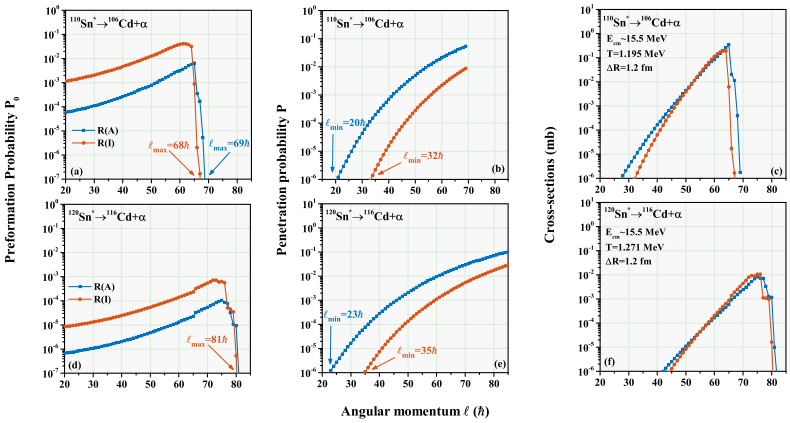

Figure 2. (a,d) Preformation probability P_0, (b,e) Penetration probability P and (c,f) cross-sections plotted in terms of angular momentum of the decaying systems ^{110}Sn* (top panels) and ^{120}Sn* (bottom panels) for the choice of mass dependent R(A) and isospin dependent R(I) radius term. The values of extreme angular momenta ℓ_{min} and ℓ_{max} are also shown.

^{110}Sn* and $\ell \simeq 23\hbar$ for ^{120}Sn*, and subsequently increases exponentially with ℓ, reflecting the reduction of the effective barrier height due to centrifugal contributions. The penetrability is plotted only up to $\ell_{\max}$. When the isospin-dependent radius $R(I)$ is employed, the onset of non-zero penetrability is shifted to higher angular momenta, starting at $\ell \simeq 32\hbar$ for ^{110}Sn* and $\ell \simeq 35\hbar$ for ^{120}Sn*. This shift arises due to the modification of the interaction potential geometry with $R(I)$, which effectively alters the barrier width and delays the opening of energetically allowed tunneling paths. As a result, the overall magnitude of the penetration probability is reduced when using $R(I)$, indicating a suppression of barrier tunneling for the emitted α particle. The decay channel cross-sections, obtained from the cumulative effect of the preformation and penetration probabilities, are shown in Figs. 2(c) and 2(f) for ^{110}Sn* and ^{120}Sn*, respectively. Although the use of $R(I)$ leads to an enhancement in the preformation probability, this effect is largely counterbalanced by the simultaneous reduction in the penetration probability. Consequently, the cross-section curves calculated using $R(A)$ and $R(I)$ nearly overlap for both isotopic systems. Only a marginal expansion of the effective angular momentum window ($\ell_{\min}$ to $\ell_{\max}$) is observed for the lighter isotope ^{110}Sn* when $R(I)$ is employed. Overall, the results indicate that while the isospin-dependent radius significantly modifies the individual DCM ingredients P_0 and P, their compensating effects lead to minimal changes in the predicted α-decay cross-sections for the systems under consideration.

Figure 3 displays the scattering potential as a function of fragment separation R for the α-decay channels (a) ^{110}Sn$^* \rightarrow {}^{106}$Cd+α and (b) ^{120}Sn$^* \rightarrow {}^{116}$Cd+α, calculated using both the mass-dependent radius $R(A)$ and the isospin-dependent radius $R(I)$. The scattering potential plays a crucial role in the DCM framework, as it governs the formation of the potential pocket, determines the barrier characteristics, and directly influences the penetration probability of the emitted cluster. A clear effect of employing the isospin-dependent radius $R(I)$ is observed for both isotopic systems. In particular, replacing $R(A)$ with $R(I)$ leads to a noticeable deepening of the potential pocket. Physically, a deeper potential pocket signifies an enhanced trapping of the preformed α cluster within the nuclear interaction region, thereby

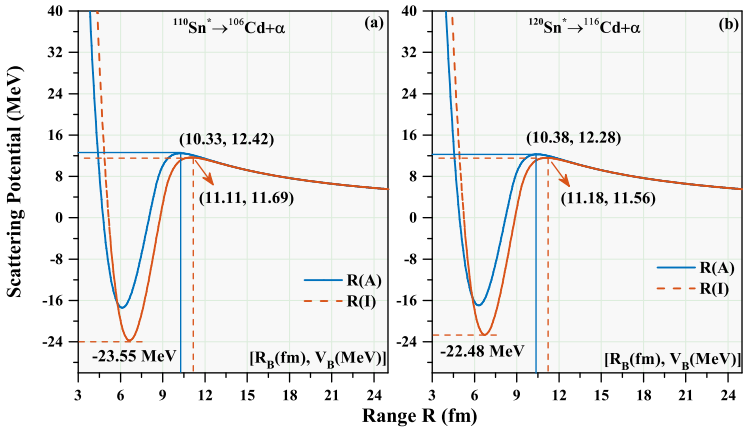

Figure 3. Scattering potential for the decay channels (a) $^{110}Sn^{*}\rightarrow^{106}Cd+\alpha$ and (b) $^{120}Sn^{*}\rightarrow^{116}Cd+\alpha$ in terms of range R(fm) parameter for the choice of mass dependent R(A) and isospin dependent R(I) radius term. The barrier position R_B and barrier height V_B is also mentioned in the figure.

increasing the stability of the cluster configuration prior to emission. This enhanced localization favors cluster formation but simultaneously modifies the tunneling conditions through the barrier by shifting the first turning point R_a from 8.44 fm to 9.04 fm for $^{110}Sn^{*}$ and 8.62 fm to 9.21 fm for the heavier isotope. Clearly, the system with higher isospin is subjected to a greater change in the first turning point. In addition to the pocket deepening, systematic shifts in both the barrier position and barrier height are observed for the two systems. For the lighter isotope $^{110}Sn^{*}$, the barrier position shifts from $R_B = 10.33$ fm to 11.11 fm, while the corresponding barrier height decreases from $V_B = 12.42$ MeV to 11.69 MeV when $R(A)$ is replaced by $R(I)$. Similarly, for the heavier isotope $^{120}Sn^{*}$, the barrier position changes from $R_B = 10.38$ fm to 11.18 fm and the barrier height reduces from $V_B = 12.28$ MeV to 11.56 MeV. These results indicate that the use of the isospin-dependent radius effectively produces a lower interaction barrier located at a larger separation distance for both isotopic systems. Such modifications in the scattering potential are consistent with the observed suppression of the penetration probability when $R(I)$ is employed and highlight the sensitivity of decay dynamics to isospin-dependent geometric effects.

Lastly, the relative impact of employing the isospin-dependent radius $R(I)$ is examined for all light particles emitted from $^{110}Sn^{*}$ in order to provide a comparative and systematic assessment of its influence across different light-particle decay channels. For this purpose, the ℓ-summed (up to the respective ℓ_{max}) preformation probability, ℓ-summed penetration probability, and the resulting ℓ-summed decay cross-sections are evaluated using both $R(A)$ and $R(I)$. The corresponding results are displayed in Fig. 4(a)–(c), respectively. It is observed that the ℓ-summed preformation probabilities of light particles exhibit only a modest sensitivity to the choice of radius parameterization. Upon replacing $R(A)$ with $R(I)$, the overall magnitude of the preformation probability changes only slightly. Interestingly, fragments with $A_L = 1$ and $A_L = 4$ display a marginal enhancement in preformation probability, whereas those with $A_L = 2$ and $A_L = 3$ show a slight reduction. This contrasting behavior can be understood in terms of the isospin structure of the emitted clusters. The $A_L = 1$ (proton) and $A_L = 4$ (α particle) clusters correspond to extreme isospin configurations, with the proton having max-

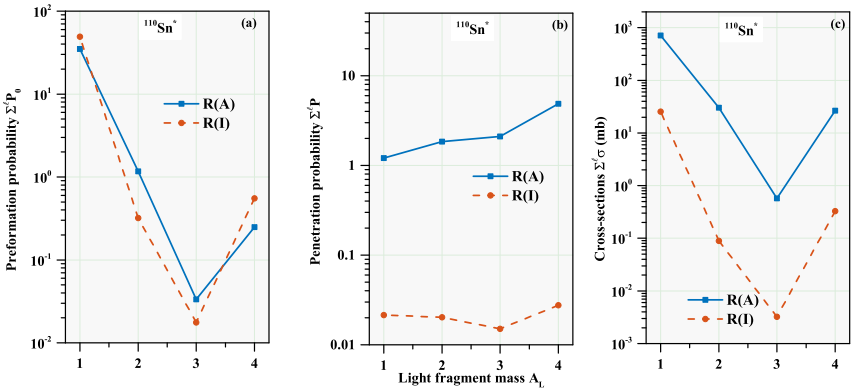

Figure 4. ℓ-summed (a) preformation probability $\Sigma^{\ell}P_0$, (b) penetration probability $\Sigma^{\ell}P$ and (c) cross-sections $\Sigma^{\ell}\sigma$ plotted in terms of light fragment mass A_L for the light particles (A_L=1-4) emerging from $^{110}Sn^*$ for the choice of mass dependent R(A) and isospin dependent R(I) radius term.

Table 1. The DCM parameters used in the present work and the corresponding barrier charactertistics i.e barrier position R_B, barrier height V_B and first turning point R_a, for the use of mass dependent R(A) and isospin dependent R(I) parameterization.

Mass dependent radius R(A)					
S. No.	Isotope	T (MeV)	R_B (fm)	V_B (MeV)	R_a (fm)
1	$^{110}Sn^*$	1.195	10.33	12.42	8.44
2	$^{120}Sn^*$	1.271	10.38	12.28	8.62
Isospin dependent radius R(I)					
S. No.	Isotope	T (MeV)	R_B (fm)	V_B (MeV)	R_a (fm)
1	$^{110}Sn^*$	1.195	11.11	11.69	9.04
2	$^{120}Sn^*$	1.271	11.18	11.56	9.21

imal isospin asymmetry and the α particle being an isospin-symmetric ($I = 0$) and strongly bound cluster. These features render their preformation relatively less sensitive to isospin-dependent geometric effects. In contrast, the $A_L = 2$ (deuteron) and $A_L = 3$ (^{3}He) clusters possess intermediate isospin characteristics, making their formation probabilities more susceptible to changes in the nuclear radius arising from isospin asymmetry. On the other hand, a pronounced reduction in magnitude is observed in the ℓ-summed penetration probabilities for all light particles when $R(I)$ is employed. This significant suppression reflects the modification of the scattering potential geometry associated with the isospin-dependent radius, which effectively increases the barrier width and delays the onset of energetically favorable tunneling paths. As a result, the probability for barrier penetration is strongly diminished for all light-particle channels. Consequently, the ℓ-summed decay cross-sections, being a cumulative effect of the preformation and penetration probabilities, exhibit a substantial overall reduction with the use of $R(I)$. This behavior indicates that although the influence of $R(I)$ on cluster preformation is relatively weak and fragment dependent, its dominant effect manifests through the suppression of barrier penetrability, leading to a significant decrease in the predicted light-particle emission cross-sections.

4 Summary and Conclusion

In conclusion, the present study systematically investigated the influence of the incorporating the isospin-dependent radius parameterization $R(I)$ on the decay properties of the $^{110,120}Sn^{*}$ isotopic systems within the Dynamical Cluster-decay Model framework. The reinstatement of the usually used mass-dependent radius $R(A)$ with $R(I)$ leads to compelling variations in the fragmentation potential landscape, identified by a reduction in its overall magnitude and a lowering of the driving potential. These structural variations decipher into an increment of the preformation probability due to reduced fragmentation potential magnitude and consequently, enhanced stability of cluster configurations. While concurrently inducing a suppression of the penetration probability resulting from the outward shift of the interaction barrier. Attributed to this cumulative behavior of preformation and penetration probability, the decay cross-sections for the decay channel under consideration i.e. α-channel remains unaffected. However, when all light-particle channels are considered altogether, the reduction of barrier penetrability poses to be the dominant effect, leading to a noticeable reduction in the decay cross-sections of the corresponding particle. Overall, the results highlight the crucial role of isospin-dependent geometric effects in governing nuclear decay processes, primarily through their strong influence on the tunneling dynamics.

Acknowledgments

The support from Department of Science and Technology, New Delhi, INDIA under the Women in Science and Engineering (WISE-PDF) scheme (No.DST/WISE-PDF/PM-15/2024) is gratefully acknowledged.

References

[1] B. B. Singh, M. K. Sharma, R. K. Gupta and W. Greiner, Int. Jour. of Mod. Phys. E **15**, 699-717 (2006).

[2] R. K. Gupta, M. Balasubramaniam, R. Kumar, D. Singh, C. Beck and W. Greiner, Phys. Rev. C **71**, 014601 (2005).

[3] C. Volant, M. Conjeaud, S. Harar et al., Phys. Lett. B **195**, 22-26 (1987).

[4] E. Gadoili, E. Gadioli Erba and M. Luinetti, Zeitschrift für Physik A Atoms and Nuclei **321**, 107-118 (1985).

[5] M. U. Khandaker, K. Kim, M. Lee, G. Kim, Physics Research Section B: Beam Interactions with Materials and Atoms **333**, 80-91 (2014).

[6] D. S. Verma, P. Chauhan and Vivek, Nucl. Phys. A **1055**, 123017 (2025).

[7] D. T. Akrawy, H. Hassanabadi, Yibin Qian, K.P. Santhosh, Nucl. Phys. A **983**, 310-320 (2019).

[8] R. A. Rebeles, A. Hermanne, S. Takács, F. Tárkányi, S. F. Kovalev, and A. Ignatyuk, Nuclear Instruments and Methods in Physics Research Section B: Beam Interactions with Materials and Atoms **260** 672-684 (2007).

[9] R. Adam Rebeles, A. Hermanne, P. Van den Winkel, F. Tárkányi, S. Takács, L. Daraban, Nuclear Instruments and Methods in Physics Research Section B: Beam Interactions with Materials and Atoms **266** 4731-4737 (2008).

[10] N. Kaur, M. Kaur, A. Kaur, S. Kaur, S. Singh and B. B. Singh, Phys. Rev. C **112** 034606 (2025).

[11] P. Mohr, G. Kiss, Z. Fülöp, D. Galaviz, G. Gyürky, and E. Somorjai, Atomic Data and Nuclear Data Tables 99, 651–679 (2013)

[12] A. Kaur and M. K. Sharma, Mod. Phys. Lett. A Vol. **33** No. **1**, 2050082 (2020).
[13] A. Kaur and M. K. Sharma, Nucl. Phy. A **957**, 274 (2017).
[14] A. Kaur, K. Sandhu, G. Sawhney and M. K. Sharma, Eur. Phys. Jour. A **58**, 59 (2022).
[15] G. Sawhney, A. Kaur, M. K. Sharma and R. K. Gupta, Phys. Rev. C **92**, 064303 (2015).
[16] R. K. Gupta *et al.*, Int. Rev. Phys. **2**, 369 (2008).
[17] M. K. Sharma, G. Sawhney, R. K. Gupta, and W. Greiner, J. Phys. G: Nucl. Part. Phys. **38**, 105101 (2011).
[18] G. Sawhney, R. Kumar, and M. K. Sharma, Phys. Rev. C **86**, 034613 (2012).
[19] G. Sawhney, G. Kaur, M. K. Sharma, and R. K. Gupta, Phys. Rev. C **88**, 034603 (2013).
[20] A. Kaur, G. Kaur, and M. K. Sharma, Nucl. Phys. A **941**, 152 (2015).
[21] H. Kröger and W. Scheid, J. Phys. G: Nucl. Part. Phys **6**, L85 (1980).
[22] P. A. Seeger, Nucl. Phys. **25**, 1 (1961).
[23] N. J. Davidson, S. S. Hsiao, J. Markram, H. G. Miller, and Y. Tzeng, Nucl. Phys. A **570** 61c (1994).
[24] W. Myers, and W. J. Swiatecki, Nucl. Phys. **81** 1 (1996).